A Systematic Study of the $\tilde{X}\ ^2B_1$, $\tilde{A}\ ^2A_1$, and $\tilde{B}\ ^2B_2$ States of the Neutral Radical PH_2

H. Lee Woodcock, Steven S. Wesolowski, Yukio Yamaguchi, and Henry F. Schaefer, III*

Center for Computational Quantum Chemistry, University of Georgia, Athens, Georgia 30602-2525

The three lowest-lying electronic states of PH_2, $\tilde{X}\ ^2B_1$, $\tilde{A}^2\ A_1$, and $\tilde{B}\ ^2B_2$, have been investigated systematically using ab initio electronic structure theory. The SCF, CASSCF, CISD, CASSCF-SOCI, CCSD, and CCSD(T) levels of theory have been employed to determine total energies, equilibrium structures, and physical properties, including dipole moments, harmonic vibrational frequencies, and infrared intensities. The predicted geometries and physical properties of the two lowest states of PH_2 are in good agreement with available experimental results. At the CCSD(T) level of theory with the correlation-consistent quadruple-ζ basis set (cc-pVQZ), the $\tilde{A}\ ^2A_1$ state of PH_2 has a large bond angle of 121.9° and is predicted to lie 52.2 kcal/mol (2.26 eV, 18 300 cm^{-1}) above the ground state. This is in excellent agreement with the experimental T_0 values of 52.26 kcal/mol (2.266 eV, 18 276.59 cm^{-1}) and 52.08 kcal/mol (2.258 eV, 18 215 cm^{-1}). The second excited electronic state ($\tilde{B}\ ^2B_2$), not studied previously, was predicted to possess an unusual acute HPH angle of 29.1° and a theoretical T_0 value of 71.3 kcal/mol (3.09 eV, 24 900 cm^{-1}) relative to the ground state.

1. Introduction

The phosphino (PH_2) radical has long been studied by experimentalists and theoreticians alike. The work put forth over the last 60 years is a testament to the chemical importance of PH_2. This importance is also demonstrated by the numerous studies performed on species isovalent to PH_2 such as CH_2[−1] and H_2O^+,[2] as well as the NH_2 molecule,[3] which has similar ground and excited-state behavior. The chemical significance of PH_2 is again presented by its role in gas-phase metal−organic chemical vapor deposition. This process, which is used in the production of III-V semiconductor materials[4] and P-doped silicon and germanium films,[5] is carried out using the hydrogen abstraction reaction

$$PH_3 + H \rightarrow PH_2 + H_2$$

It has also been proposed by Lee et al.[6] that this reaction plays a role in forming the final product [P_4(s)] of the dehydrogenation of phosphine (PH_3), which is predicted to contribute to the great red spot on Jupiter.[7]

In 1956, Ramsay[8] published the first paper characterizing the electronic spectrum of the free radical PH_2. In this work, using flash photolysis of phosphine, Ramsay was able to determine the absorption of PH_2 at about 5500 Å. Later experiments[9−11] explored the structure and properties of different states and concluded that there is a $^2B_1 \rightarrow\ ^2A_1$ transition from the ground state to the first excited electronic state. These absorption experiments and emission experiments helped researchers accurately determine the origin of the ν_2 band located at 1102 cm^{-1}.[9−11]

Over the years, there have been many theoretical and experimental studies performed in order to gain insight into the $\tilde{X}\ ^2B_1 \rightarrow \tilde{A}\ ^2A_1$ transition. Most of these studies have primarily focused on the ν_2 (bending) mode by adding successive quanta to the upper electronic state. A large amount of attention has been paid to the unusual nature of the vibrational intervals of the ν_2 band in the $^2A_1$ state. Ramsay[8] interpreted the anomalous behavior of this mode to be due to the repulsive forces of the hydrogens as bending occurs. Dixon[12] has also studied the vibrational intervals and disagreed with Ramsay on the origin of the anomaly. A theoretical study undertaken in 1977 by So and Richards[13] supported Dixon's conclusion that the vibrational interval anomaly is attributed to a barrier in the potential function analogous to the ν_2 bending mode.

There have also been numerous experimental and theoretical studies that investigate the energetics and/or geometrical parameters of PH_2. The three earliest theoretical studies are the 1977 So and Richards[13] Hartree−Fock study of the $\tilde{X}\ ^2B_1$ and $\tilde{A}\ ^2A_1$ states of PH_2, the 1978 Ball and Thomson[14] Hartree−Fock paper on SiH_2, PH_2, and their ionic analogues, and the 1979 Peric, Buenker, and Peyerimhoff[15] study of the $^2A_1-^2B_1$ transition of PH_2, which made use of the MRD-CI method in conjunction with fitting to experimental data. Peric's study[15] predicted the equilibrium P−H distances of the $\tilde{X}\ ^2B_1$ and $\tilde{A}\ ^2A_1$ states to be 1.420 and 1.399 Å and the HPH bond angles of these states to be 91.1° and 122.1°, respectively. More recent theoretical studies have been performed on PH_2. In 1988, Alberts and Handy[16] made use of UMP3 gradients to obtain geometrical parameters for the $\tilde{X}\ ^2B_1$ state. Likewise, the MCSCF study by Pope, Hillier, and Guest[17] examined the ground-state geometry.

The important experimental studies performed to determine the structures of the $\tilde{X}\ ^2B_1$ and $\tilde{A}\ ^2A_1$ states are as follows: the 1966 study by Herzberg;[18] the 1972 study by Berthou;[19] and the 1998 work by Hirao, Hayakashi, Yamamoto, and Saito,[20] in which they determined the P−H distance (r_0) and HPH bond angle (θ_0) of the $\tilde{X}\ ^2B_1$ state to be 1.4260 Å and 91.65°, respectively. Berthou[19] determined the P−H distance of the $\tilde{X}$ and $\tilde{A}$ state to be 1.418 and 1.389 Å and the HPH bond angle to be 91.7° and 123.2°, respectively.

Both Herzberg[18] and Berthou[19] reported the vibrational frequencies of the $\tilde{X}$ and $\tilde{A}$ states of PH_2. Peric's multireference CI study[15] predicted $\upsilon_1 = 2330$, $\upsilon_2 = 1110$, $\upsilon_3 = 2495$ as vibrational frequencies (in cm^{-1}) for the $\tilde{X}\ ^2B_1$ state and $\upsilon_1 = 2430$, $\upsilon_2 = 973$, $\upsilon_3 = 2660$ for the $\tilde{A}\ ^2A_1$ state. This theoretical work compares very nicely with the following experimental results: $\upsilon_1 = 2310$[21] and $\upsilon_2 = 1103$[22] for the $\tilde{X}\ ^2B_1$ state and $\upsilon_2 = 949$[21−23] for the $\tilde{A}\ ^2A_1$ state. The aforementioned work shows that quantum chemical methods can not only accurately predict

10.1021/jp0042258 CCC: $20.00
Published on Web 04/27/2001

vibrational frequencies, but they can also give experimentalists a good indication of where the unknowns bands lie. The most accurate theoretical prediction of T_0 to date was reported by Peric et al.[15] to be 18760 cm^{-1}, which was compared favorably with the experimental T_0 values, 18 277 cm^{-1}[18, 22] and 18 215 cm^{-1}.[23, 24]

The objective of the present study is to systematically examine the ground and first two excited electronic states of PH_2 using ab initio self-consistent field (SCF), configuration interaction (CISD), complete active space (CASSCF and CASSCF-SOCI), and coupled cluster [CCSD and CCSD(T)] wave functions with a wide variety of basis sets. This study is analogous to work previously done in our laboratory on NH_2[3] and PH_2^+,[25] in which theoretically predicted energy separations between the ground and excited states (as well as geometrical parameters) were found to be in excellent agreement with those of the experiment. Also, the progression in levels of theory as well as in basis set size shown in our study provides a means for estimation of molecular properties and energetics within chemical accuracy (1 kcal/mol, 350 cm^{-1}) when larger basis sets and higher levels of theory cannot be employed. In addition to providing highly accurate structures, energy separations, and harmonic vibrational frequencies for the ground and first excited states, the present study also provides the first exploration of the $\tilde{B}\ ^2B_2$ state of PH_2. The $\tilde{B}\ ^2B_2$ state is investigated to elucidate the nature of its unusual acute bond angle as well as to compare with the properties of the previously studied $\tilde{B}\ ^2B_2$ state of NH_2.[3]

2. Theoretical Procedures

Eleven basis sets were used in this study. Eight of these basis sets were of triple-ζ (TZ) quality, while the remaining three were correlation-consistent basis sets of double-ζ (cc-pVDZ), triple-ζ (cc-pVTZ), and quadruple-ζ (cc-pVQZ) quality. The TZ basis for the phosphorus atom was derived from McLean and Chandler's TZ contraction[26] of Huzinaga's primitive Gaussian functions[27] and is designated (12s9p/6s5p). The TZ basis set for the hydrogen atom was obtained from Dunning's TZ contraction[28] of Huzinaga's primitive Gaussian functions[29] and is designated (5s/3s). The orbital exponents of the polarization functions were $\alpha_d(P) = 1.20$ and 0.300 and $\alpha_p(H) = 1.50$ and 0.375 for double polarization (TZ2P) and $\alpha_d(P) = 2.40$, 0.600, and 0.150 and $\alpha_p(H) = 3.00$, 0.750, and 0.1875 for triple polarization (TZ3P). Five d-like and seven f-like pure angular momentum functions were used throughout.

The orbital exponents of the higher angular momentum functions were $\alpha_f(P) = 0.450$ and $\alpha_d(H) = 1.00$ for a single set of higher angular momentum functions [TZ2P(f,d)] and $\alpha_f(P) = 0.900$ and 0.225 and $\alpha_d(H) = 2.00$ and 0.500 for double sets of higher angular momentum functions [TZ3P(2f,2d)]. The diffuse function orbital exponents were determined in an "even-tempered sense" as a mathematical extension of the primitive set according to the formula of Lee and Schaefer,[30] with $\alpha_s(P) = 0.034\ 63$, $\alpha_p(P) = 0.031\ 38$, and $\alpha_s(H) = 0.030\ 16$ for single diffuse functions [TZ2P+diff and TZ2P(f,d)+diff] and $\alpha_s(P) = 0.034\ 63$ and $0.011\ 11$, $\alpha_p(P) = 0.031\ 38$ and $0.011\ 61$, and $\alpha_s(H) = 0.030\ 16$ and $0.009\ 247$ for double diffuse functions [TZ3P+2diff and TZ3P(2f,2d)+2diff]. The largest TZ plus basis set, TZ3P(2f,2d)+2diff, contained 119 contracted Gaussian functions with a contraction scheme of (14s11p3d2f/8s7p3d2f) for the phosphorus atom and (7s3p2d/5s3p2d) for the hydrogen atom.

We also employed three correlation-consistent basis sets (cc-pVXZ; X = D, T, or Q) in addition to the eight TZ type basis sets. These basis sets were optimized by Dunning for hydrogen,[31] and Woon and Dunning for phosphorus.[32] The cc-pVQZ basis sets for the hydrogen and phosphorus atoms are designated by the contraction schemes (6s3p2d1f/4s3p2d1f) and (16s11p3d2f1g/6s5p3d2f1g), respectively.

The geometries of the lowest three electronic states were optimized via standard analytic derivative methods[33−35] at the SCF and CISD levels of theory, while finite differences of energy points were used to optimize structures at the couple cluster with single and double excitations (CCSD)[36] and CCSD with perturbative triples [CCSD(T)][37] levels of theory. The implementations of the open-shell CCSD and CCSD(T) methods used were those of Scuseria.[38] Complete active space (CAS)-SCF[39−41] and CASSCF second-order configuration interaction (SOCI)[42] levels of theory were also utilized to assess relative energies. Harmonic vibrational frequencies and associated infrared (IR) intensities were determined analytically for the lowest three states at the SCF level of theory.[43−46] Harmonic frequencies were obtained by finite differences of analytic gradients at the CISD[47−50] level of theory and via five-point numerical differentiation of the energies for the CCSD and CCSD(T) methods. Geometrical parameters (bond lengths and bond angles) obtained by energy point optimizations are comparable to analytically optimized parameters to at least 10^{-7} hartree/bohr, and vibrational frequencies are converged to within 0.1 cm^{-1}.[51] For all methods, the energies and Cartesian gradients were optimized to at least 10^{-12} and 10^{-6} au, respectively.

In the CISD, CCSD, and CCSD(T) procedures with the TZ plus quality basis sets, the five core (P 1s, 2s, and 2p) orbitals were frozen, and one highest-lying virtual (P 1s*) orbital was deleted. With the three correlation-consistent basis sets, the aforementioned correlated procedures were performed by freezing the five core orbitals only.

CASSCF wave functions were constructed at the CISD geometries with the corresponding basis set, and the resulting orbitals were used to determine energies at the CISD level (CASSCF-SOCI). The active space used was comprised of seven electrons in eight molecular orbitals and is denoted ($7e^-$/8 MO). This active space provided 588 CSFs (configuration state functions) ($\tilde{X}\ ^2B_1$), 616 CSFs ($\tilde{A}\ ^2A_1$), and 588 CSFs ($\tilde{B}\ ^2B_2$) for the CASSCF procedure. In all CASSCF-SOCI computations, the five core orbitals were frozen and one highest-lying virtual orbital was deleted. With the largest basis set used [TZ3P(2f,-2d)], SOCI wave functions consisted of 20 64 412 CSFs ($\tilde{X}\ ^2B_1$), 20 67 272 CSFs ($\tilde{A}\ ^2A_1$), and 20 66 204 CSFs ($\tilde{B}\ ^2B_2$). All computations were performed using the PSI 2.0.8 suite of ab initio quantum mechanical programs.[52]

3. Electronic Structure Considerations

The $\tilde{X}\ ^2B_1$ electronic state of PH_2 molecule is bent with C_{2v} symmetry and is analogous to the $\tilde{X}$ state of NH_2. The electron configuration of this state may be expressed as

$$[\text{core}](4a_1)^2(2b_2)^2(5a_1)^2(2b_1)^1 \qquad \tilde{X}\ ^2B_1$$

where

$$[\text{core}] = (1a_1)^2(2a_1)^2(1b_2)^2(3a_1)^2(1b_1)^2$$

The first excited state, $\tilde{A}\ ^2A_1$, also is of C_{2v} symmetry, with a significantly more obtuse H−P−H bond angle and can be represented as

$$[\text{core}](4a_1)^2(2b_2)^2(5a_1)^1(2b_1)^2 \qquad \tilde{A}\ ^2A_1$$

TABLE 1: Theoretical Predictions of the Total Energy (in hartree), Bond Length (in Å), Bond Angle (in deg), Dipole Moment (in debye), Harmonic Vibrational Frequencies (in cm^{-1}), Infrared Intensities (in parentheses in km/mol), and Zero-Point Vibrational Energy (in kcal/mol) for the $\tilde{X}\ ^2B_1$ State of the PH_2 Molecule at the SCF and CISD Levels of Theory

level of theory	energy	r_e	θ_e	μ_e	$\omega_1(a_1)$	$\omega_2(a_1)$	$\omega_3(b_2)$	ZPVE
TZ2P SCF	−341.876130	1.4083	93.57	0.724	2500(68.4)	1227(26.5)	2498(101.6)	8.90
TZ2P+diff SCF	−341.876637	1.4079	93.60	0.754	2501(69.4)	1226(37.2)	2501(97.1)	8.90
TZ3P SCF	−341.877996	1.4073	93.63	0.673	2526(60.3)	1229(26.3)	2526(88.5)	8.98
TZ3P+2diff SCF	−341.878229	1.4072	93.67	0.686	2526(61.8)	1227(29.7)	2526(87.4)	8.98
TZ2P(f,d) SCF	−341.877766	1.4088	93.61	0.713	2514(70.6)	1226(27.0)	2511(104.2)	8.94
TZ2P(f,d)+diff SCF	−341.878317	1.4084	93.66	0.744	2516(71.5)	1225(38.2)	2514(98.7)	8.94
TZ3P(2f,2d) SCF	−341.879130	1.4075	93.66	0.673	2517(61.5)	1226(27.2)	2517(88.9)	8.95
TZ3P(2f,2d)+2diff SCF	−341.879343	1.4074	93.71	0.683	2518(62.7)	1224(30.4)	2518(87.9)	8.95
cc-pVDZ SCF	−341.867608	1.4218	93.47	0.755	2510(74.4)	1216(27.4)	2512(120.1)	8.92
cc-pVTZ SCF	−341.881631	1.4115	93.63	0.699	2510(66.7)	1222(27.1)	2511(101.4)	8.92
cc-pVQZ SCF	−341.885889	1.4087	93.72	0.691	2514(63.8)	1223(28.8)	2514(92.1)	8.94
TZ2P CISD	−342.018635	1.4160	91.84	0.574	2399(63.6)	1154(23.1)	2404(88.4)	8.52
TZ2P+diff CISD	−342.019287	1.4156	91.81	0.598	2401(64.5)	1154(31.0)	2406(85.3)	8.52
TZ3P CISD	−342.022066	1.4139	92.14	0.500	2438(55.3)	1165(21.6)	2442(74.9)	8.64
TZ3P+2diff CISD	−342.022524	1.4139	92.13	0.512	2438(56.4)	1164(24.3)	2441(73.7)	8.64
TZ2P(f,d) CISD	−342.036535	1.4152	92.15	0.629	2434(56.7)	1153(22.1)	2435(80.7)	8.61
TZ2P(f,d)+diff CISD	−342.037143	1.4149	92.14	0.652	2435(57.5)	1154(30.2)	2437(77.0)	8.61
TZ3P(2f,2d) CISD	−342.041001	1.4136	92.17	0.562	2441(49.1)	1156(20.7)	2447(67.5)	8.64
TZ3P(2f,2d)+2diff CISD	−342.041325	1.4136	92.20	0.570	2442(50.0)	1155(23.1)	2448(66.7)	8.64
cc-pVDZ CISD	−341.999911	1.4319	92.04	0.646	2422(70.0)	1148(22.9)	2429(102.0)	8.58
cc-pVTZ CISD	−342.042849	1.4177	92.24	0.620	2432(52.8)	1150(20.9)	2439(76.1)	8.61
cc-pVQZ CISD	−342.054740	1.4146	92.29		2443	1152	2448	8.64
experimental (r_0 and θ_0 values)		1.428[18]	91.5[18]					
experimental (r_0 and θ_0 values)		1.418[19]	91.7[19]					
experimental (r_0 and θ_0 values)		1.4260[20]	91.65[20]					
experimental (ν values)					2310[22]	1102[18]		
experimental (ν values)					2270[61]	1103[23]		

The final state studied, $\tilde{B}\ ^2B_2$, follows the C_{2v} symmetry trend but has substantial geometrical differences from the $\tilde{X}\ ^2B_1$ and $\tilde{A}\ ^2A_1$ states. The second excited state may be expressed as

$$[\text{core}]\ (4a_1)^2(2b_2)^1(5a_1)^2(2b_1)^2 \qquad \tilde{B}\ ^2B_2$$

Consistent with the Walsh diagram[53] for AH_2 systems, the singly occupied $2b_1$ orbital does not contribute significantly to the bent nature of the $\tilde{X}\ ^2B_1$ ground state. However, the doubly occupied $5a_1$ orbital is strongly stabilized by bending. The $\tilde{A}\ ^2A_1$ state has a doubly occupied $2b_1$ orbital and a singly occupied $5a_1$ orbital, which lead to a much more obtuse H−P−H bond angle. Lastly, the $\tilde{B}\ ^2B_2$ state is characterized by an extremely acute H−P−H bond angle, which is a result of the excitation of an electron out of the predominantly P−H bonding $2b_2$ orbital into the nonbonding $2b_1$ orbital.

It is important to characterize the nature of the SCF reference wave functions in the correlated procedures—especially for the investigations of the excited states. In earlier work, we extended the stability analysis of an SCF wave function to general open-shell SCF wave functions.[54] In that method, the number of negative eigenvalues of the molecular orbital (MO) Hessian matrix (the second derivative matrix of the SCF energy with respect to the changes in the molecular orbitals at the fixed geometry) is termed "an instability" index. According to our stability analysis, the $\tilde{X}\ ^2B_1$ state showed an instability index of zero. Thus, the physical properties for the ground state determined from correlated wave functions based on the SCF wave function should be reliable. However, the first excited state ($\tilde{A}\ ^2A_1$) presents an instability index of one. The eigenvector associated with the negative eigenvalue involves a ($5a_1$) → ($2b_1$) MO rotation. This implies that there is one lower-lying state ($\tilde{X}\ ^2B_1$) at the equilibrium geometry of the first excited state. The second eigenvalue is positive, with the eigenvector involving a ($5a_1$) → ($2b_2$) MO rotation. Therefore, the $\tilde{B}\ ^2B_2$ state lies above the $\tilde{A}\ ^2A_1$ state at this geometry. Although the $\tilde{A}\ ^2A_1$ state of the SCF wave function is unstable with respect to MO rotation, the asymmetric stretching frequency may be determined appropriately due to the orthogonality of the first two states in C_s symmetry ($\tilde{X}\ 1^2A''$ and $\tilde{A}\ 1^2A'$).

The instability index of the second excited state ($\tilde{B}\ ^2B_2$) of PH_2 is also found to be 1. The eigenvector associated with the negative eigenvalue involves a ($2b_2$) → ($2b_1$) MO rotation. This indicates that the SCF wave function is unstable and there is one lower-lying state ($\tilde{X}\ ^2B_1$) at the equilibrium geometry of the second excited state. The MO Hessian eigenvalue with the eigenvector involving a ($2b_2$) → ($5a_1$) MO rotation is positive. Thus, the $\tilde{A}\ ^2A_1$ state lies above the $\tilde{B}\ ^2B_2$ state. Even though the $\tilde{B}\ ^2B_2$ state of the SCF wave function is unstable, the asymmetric stretching frequency may be obtained without variational collapse at the equilibrium geometry due to the large geometrical differences observed between the $\tilde{X}\ ^2B_1$ state and $\tilde{B}\ ^2B_2$ state. Therefore, the physical properties of the three electronic states of PH_2 treated in this research may be determined correctly in the variational sense with all correlated methods as well as the SCF method at their equilibrium geometries.

4. Results and Discussion

The three lowest-lying electronic states of the PH_2 molecule have bent equilibrium structures with C_{2v} symmetry. Tables 1 and 2 contain total energies, equilibrium geometries, dipole moments (Table 1 only), harmonic vibrational frequencies with their respective IR intensities (Table 1 only), and zero-point vibrational energies (ZPVEs) for the ground state ($\tilde{X}\ ^2B_1$) predicted at 44 levels of theory. Tables 3 and 4 provide the corresponding quantities for the first ($\tilde{A}\ ^2A_1$) excited state and Tables 5 and 6 for the second ($\tilde{B}\ ^2B_2$) excited state. Table 7 presents the CASSCF and CASSCF-SOCI energies at the CISD-optimized geometries for the three states. Tables 8 and 9 contain the relative energies of the first two excited states with respect to the ground state at the SCF, CISD, CASSCF, CASSCF-SOCI, CCSD, and CCSD(T) levels of theory. The ZPVE corrected

TABLE 2: Theoretical Predictions of the Total Energy (in hartree), Bond Length (in Å), Bond Angle (in deg), Harmonic Vibrational Frequencies (in cm^{-1}), and Zero-Point Vibrational Energy (in kcal/mol) for the $\tilde{X}\ ^2B_1$ State of the PH_2 Molecule at the CCSD and CCSD(T) Levels of Theory

level of theory	energy	r_e	θ_e	$\omega_1(a_1)$	$\omega_2(a_1)$	$\omega_3(b_2)$	ZPVE
TZ2P CCSD	−342.025369	1.4190	91.67	2371	1142	2378	8.42
TZ2P+diff CCSD	−342.026047	1.4186	91.63	2373	1142	2379	8.43
TZ3P CCSD	−342.028971	1.4167	92.00	2412	1154	2416	8.55
TZ3P+2diff CCSD	−342.029451	1.4167	91.99	2411	1153	2415	8.55
TZ2P(f,d) CCSD	−342.044313	1.4182	92.00	2406	1141	2408	8.51
TZ2P(f,d)+diff CCSD	−342.044944	1.4180	91.97	2408	1142	2410	8.52
TZ3P(2f,2d) CCSD	−342.049085	1.4166	92.01	2414	1144	2421	8.55
TZ3P(2f,2d)+2diff CCSD	−342.049419	1.4166	92.04	2415	1143	2421	8.55
cc-pVDZ CCSD	−342.005704	1.4347	91.91	2397	1138	2406	8.49
cc-pVTZ CCSD	−342.050817	1.4208	92.09	2404	1137	2412	8.51
cc-pVQZ CCSD	−342.063184	1.4177	92.13	2415	1139	2421	8.54
TZ2P CCSD(T)	−342.029456	1.4208	91.45	2361	1140	2366	8.39
TZ2P+diff CCSD(T)	−342.030166	1.4204	91.41	2363	1141	2368	8.39
TZ3P CCSD(T)	−342.033399	1.4187	91.79	2400	1152	2404	8.51
TZ3P+2diff CCSD(T)	−342.033908	1.4187	91.78	2399	1151	2403	8.51
TZ2P(f,d) CCSD(T)	−342.049729	1.4202	91.74	2395	1139	2396	8.48
TZ2P(f,d)+diff CCSD(T)	−342.050379	1.4199	91.72	2396	1140	2398	8.48
TZ3P(2f,2d) CCSD(T)	−342.055074	1.4188	91.76	2401	1142	2408	8.51
TZ3P(2f,2d)+2diff CCSD(T)	−342.055424	1.4188	91.79	2402	1141	2408	8.51
cc-pVDZ CCSD(T)	−342.008622	1.4365	91.75	2381	1129	2392	8.44
cc-pVTZ CCSD(T)	−342.056502	1.4229	91.86	2387	1125	2396	8.45
cc-pVQZ CCSD(T)	−342.069714	1.4200	91.87	2396	1125	2404	8.47
experimental (r_0 and θ_0 values)		1.428[18]	91.5[18]				
experimental (r_0 and θ_0 values)		1.418[19]	91.7[19]				
experimental (r_0 and θ_0 values)		1.4260[20]	91.65[20]				
experimental (ν values)				2310[22]	1102[18]		
experimental (ν values)				2270[61]	1103[23]		

TABLE 3: Theoretical Predictions of the Total Energy (in hartree), Bond Length (in Å), Bond Angle (in deg), Dipole Moment (in debye), Harmonic Vibrational Frequencies (in cm^{-1}), Infrared Intensities (in parentheses in km/mol), and Zero-Point Vibrational Energy (in kcal/mol) for the $\tilde{A}\ ^2A_1$ State of the PH_2 Molecule at the SCF and CISD Levels of Theory

level of theory	energy	r_e	θ_e	μ_e	$\omega_1(a_1)$	$\omega_2(a_1)$	$\omega_3(b_2)$	ZPVE
TZ2P SCF	−341.789608	1.3823	122.12	0.345	2605(4.6)	1062(12.1)	2690(3.5)	9.09
TZ2P+diff SCF	−341.790244	1.3821	122.21	0.382	2606(4.3)	1062(15.2)	2691(4.4)	9.09
TZ3P SCF	−341.791224	1.3822	122.05	0.354	2624(3.0)	1063(12.1)	2709(3.2)	9.14
TZ3P+2diff SCF	−341.791760	1.3822	122.07	0.366	2624(3.0)	1062(12.8)	2709(3.7)	9.14
TZ2P(f,d) SCF	−341.792008	1.3830	122.11	0.362	2615(4.6)	1060(11.1)	2699(3.3)	9.11
TZ2P(f,d)+diff SCF	−341.792595	1.3829	122.21	0.400	2615(4.3)	1060(14.1)	2699(4.3)	9.11
TZ3P(2f,2d) SCF	−341.793251	1.3822	122.19	0.368	2617(3.4)	1061(11.2)	2702(4.3)	9.12
TZ3P(2f,2d)+2diff SCF	−341.793723	1.3822	122.22	0.380	2617(3.5)	1060(12.1)	2702(4.9)	9.12
cc-pVDZ SCF	−341.779282	1.3934	122.20	0.406	2612(5.5)	1048(11.9)	2702(1.0)	9.10
cc-pVTZ SCF	−341.795392	1.3851	122.27	0.392	2610(3.6)	1056(11.1)	2697(2.7)	9.10
cc-pVQZ SCF	−341.800199	1.3830	122.25	0.382	2615(3.7)	1061(11.6)	2700(4.3)	9.11
TZ2P CISD	−341.932614	1.3880	121.76	0.331	2510(3.5)	1009(9.3)	2605(2.3)	8.76
TZ2P+diff CISD	−341.933415	1.3879	121.75	0.364	2510(3.3)	1008(11.7)	2604(2.9)	8.75
TZ3P CISD	−341.936366	1.3878	121.70	0.319	2535(2.2)	997(9.6)	2626(2.5)	8.80
TZ3P+2diff CISD	−341.937060	1.3880	121.70	0.331	2534(2.3)	996(10.3)	2625(3.0)	8.80
TZ2P(f,d) CISD	−341.951305	1.3892	121.74	0.370	2528(4.6)	997(7.4)	2616(3.4)	8.78
TZ2P(f,d)+diff CISD	−341.951964	1.3893	121.73	0.403	2527(4.4)	995(9.6)	2615(4.2)	8.77
TZ3P(2f,2d) CISD	−341.956307	1.3890	121.90	0.353	2529(3.5)	997(7.5)	2620(4.9)	8.79
TZ3P(2f,2d)+2diff CISD	−341.956835	1.3891	121.93	0.364	2529(3.5)	997(8.2)	2619(5.5)	8.78
cc-pVDZ CISD	−341.911399	1.4017	121.93	0.411	2527(3.9)	980(8.1)	2621(0.4)	8.76
cc-pVTZ CISD	−341.957734	1.3914	122.07	0.402	2524(3.8)	989(7.3)	2617(3.6)	8.76
cc-pVQZ CISD	−341.970722	1.3897	121.98		2531	994	2621	8.79
experimental (r_0 and θ_0 values)		1.399[18]	123.1[18]					
experimental (r_0 and θ_0 values)		1.389[19]	123.2[19]					
experimental (ν value)						949[22−24]		

energy separations (T_0 values) were determined using respective harmonic vibrational frequencies at the same level of theory. For CASSCF and CASSCF-SOCI energy separations, the corresponding CISD ZPVE values were utilized.

A. Geometries. There have been three major experimental efforts designed to elucidate the structure of PH_2. The first study was undertaken by Herzberg[18] in 1966 and yielded $r_0 = 1.428$ Å and $\theta_0 = 91.5°$ for the $\tilde{X}\ ^2B_1$ state as well as $r_0 = 1.399$ Å and $\theta_0 = 123.1°$ for the $\tilde{A}\ ^2A_1$ state. The next experimental effort was put forth by Berthou[19] in 1971 and resulted in $r_0 = 1.418$ Å and $\theta_0 = 91.7°$ for the $\tilde{X}\ ^2B_1$ state and $r_0 = 1.389$ Å and $\theta_0 = 123.2°$ for the $\tilde{A}\ ^2A_1$ state. The most recent and most accurate study is the microwave spectroscopic study performed by Hirao et al.[20] in 1998; they found an r_0 of 1.4260 Å and θ_0 of 91.65° for the $\tilde{X}$ state only.

In addition to the above experimental studies, numerous theoretical efforts have been made to predict structures for PH_2. Three of the earliest were a 1977 minimal basis set SCF study by So and Richards,[13] a 1979 UHF study by Hinchcliffe and Bounds,[55] and the 1979 work of Peric et al.[15] that used MRD-CI and fitting methods[56] to arrive at bond lengths of 1.420 and 1.399 Å as well as θ_e values of 91.1° and 122.1° for the $\tilde{X}$ and

TABLE 4: Theoretical Predictions of the Total Energy (in hartree), Bond Length (in Å), Bond Angle (in deg), Harmonic Vibrational Frequencies (in cm^{-1}), and Zero-Point Vibrational Energy (in kcal/mol) for the $\tilde{A}\ ^2A_1$ State of the PH_2 Molecule at the CCSD and CCSD(T) Levels of Theory

level of theory	energy	r_e	θ_e	$\omega_1(a_1)$	$\omega_2(a_1)$	$\omega_3(b_2)$	ZPVE
TZ2P CCSD	−341.939559	1.3905	121.67	2485	998	2581	8.67
TZ2P+diff CCSD	−341.940413	1.3904	121.64	2484	996	2580	8.66
TZ3P CCSD	−341.943681	1.3903	121.59	2510	985	2602	8.72
TZ3P+2diff CCSD	−341.944407	1.3905	121.59	2508	983	2600	8.71
TZ2P(f,d) CCSD	−341.959290	1.3920	121.64	2500	984	2590	8.68
TZ2P(f,d)+diff CCSD	−341.959997	1.3921	121.60	2499	982	2589	8.68
TZ3P(2f,2d) CCSD	−341.964808	1.3919	121.79	2501	984	2593	8.69
TZ3P(2f,2d)+2diff CCSD	−341.965360	1.3920	121.82	2501	983	2593	8.69
cc-pVDZ CCSD	−341.917186	1.4040	121.87	2505	969	2602	8.69
cc-pVTZ CCSD	−341.966017	1.3943	121.97	2496	976	2591	8.67
cc-pVQZ CCSD	−341.979592	1.3927	121.87	2502	980	2594	8.69
TZ2P CCSD(T)	−341.943832	1.3920	121.65	2475	996	2571	8.64
TZ2P+diff CCSD(T)	−341.944753	1.3919	121.60	2475	995	2570	8.63
TZ3P CCSD(T)	−341.948522	1.3921	121.57	2498	983	2590	8.68
TZ3P+2diff CCSD(T)	−341.949298	1.3924	121.57	2496	982	2588	8.67
TZ2P(f,d) CCSD(T)	−341.965106	1.3937	121.64	2489	982	2579	8.65
TZ2P(f,d)+diff CCSD(T)	−341.965859	1.3938	121.58	2488	981	2578	8.64
TZ3P(2f,2d) CCSD(T)	−341.971471	1.3940	121.79	2487	982	2580	8.65
TZ3P(2f,2d)+2diff CCSD(T)	−341.972050	1.3941	121.82	2487	981	2579	8.65
cc-pVDZ CCSD(T)	−341.920051	1.4053	121.86	2491	962	2597	8.65
cc-pVTZ CCSD(T)	−341.972185	1.3961	121.98	2479	965	2576	8.61
cc-pVQZ CCSD(T)	−341.986796	1.3948	121.88	2483	968	2584	8.63
experimental (r_0 and θ_0 values)		1.399[18]	123.1[18]				
experimental (r_0 and θ_0 values)		1.389[19]	123.2[19]				
experimental (ν value)					949[22−24]		

TABLE 5: Theoretical Predictions of the Total Energy (in hartree), Bond Length (in Å), Bond Angle (in deg), P···H_2 Length (in Å), Dipole Moment (in debye), Harmonic Vibrational Frequencies (in cm^{-1}), Infrared Intensities (in parentheses in km/mol), and Zero-Point Vibrational Energy (in kcal/mol) for the $\tilde{B}\ ^2B_2$ State of the PH_2 Molecule at the SCF and CISD Levels of Theory

level of theory	energy	r_e	$r_{P\cdots H_2}$	θ_e	μ_e	$\omega_1(a_1)$	$\omega_2(a_1)$	$\omega_3(b_2)$	ZPVE
TZ2P SCF	−341.755607	1.9318	1.8939	22.75	1.362	4137(69.9)	335(68.9)	1036(10.3)	7.87
TZ2P+diff SCF	−341.756463	1.9136	1.8751	23.03	1.400	4108(66.9)	360(67.9)	1063(10.8)	7.91
TZ3P SCF	−341.756213	1.8410	1.8002	24.17	1.359	3994(39.0)	399(51.4)	1178(14.8)	7.96
TZ3P+2diff SCF	−341.756892	1.8324	1.7912	24.32	1.379	3976(37.3)	417(50.0)	1192(14.2)	7.99
TZ2P(f,d) SCF	−341.757627	1.8679	1.8281	23.71	1.486	4043(52.8)	396(67.8)	1144(11.2)	7.98
TZ2P(f,d)+diff SCF	−341.758533	1.8527	1.8123	23.97	1.517	4012(49.1)	423(65.6)	1172(11.2)	8.02
TZ3P(2f,2d) SCF	−341.758913	1.8147	1.7729	24.62	1.431	3941(32.9)	463(46.8)	1239(14.1)	8.07
TZ3P(2f,2d)+2diff SCF	−341.759499	1.8096	1.7677	24.72	1.444	3930(32.2)	476(45.3)	1249(13.5)	8.08
cc-pVDZ SCF	−341.747244	1.9528	1.9146	22.70	1.380	4217(53.4)	351(85.1)	1035(8.3)	8.01
cc-pVTZ SCF	−341.762227	1.8570	1.8168	23.89	1.444	4026(45.4)	418(61.6)	1171(12.1)	8.03
cc-pVQZ SCF	−341.766497	1.8250	1.7837	24.42	1.453	3964(37.0)	463(51.7)	1232(12.9)	8.09
TZ2P CISD	−341.898646	1.7122	1.6640	27.26	1.597	3445(0.0)	713(19.7)	1328(8.5)	7.84
TZ2P+diff CISD	−341.899693	1.7109	1.6625	27.31	1.604	3437(0.0)	721(19.1)	1331(7.2)	7.85
TZ3P CISD	−341.902530	1.6764	1.6262	28.11	1.434	3349(0.7)	836(10.6)	1453(9.3)	8.06
TZ3P+2diff CISD	−341.903544	1.6756	1.6253	28.14	1.438	3345(0.6)	843(10.0)	1451(7.9)	8.06
TZ2P(f,d) CISD	−341.917993	1.6798	1.6296	28.09	1.672	3338(0.6)	821(15.7)	1448(8.2)	8.02
TZ2P(f,d)+diff CISD	−341.918968	1.6787	1.6283	28.14	1.676	3330(0.7)	829(15.0)	1453(6.6)	8.02
TZ3P(2f,2d) CISD	−341.923386	1.6636	1.6124	28.50	1.498	3293(0.6)	890(8.0)	1496(8.4)	8.12
TZ3P(2f,2d)+2diff CISD	−341.924080	1.6632	1.6120	28.52	1.500	3290(0.6)	894(7.4)	1497(7.4)	8.12
cc-pVDZ CISD	−341.877768	1.7495	1.7016	26.89	1.689	3570(0.0)	677(37.1)	1295(5.0)	7.92
cc-pVTZ CISD	−341.925574	1.6832	1.6332	28.00	1.620	3357(0.2)	833(16.1)	1456(8.0)	8.07
cc-pVQZ CISD	−341.938052	1.6667	1.6157	28.43		3302	888	1507	8.14

$\tilde{A}$ states, respectively. A more recent study by Alberts and Handy[16] made use of the UMP3 method and a 11*s*8*p*3d/6*s*3p basis set to arrive at r_e and θ_e values of 1.414 Å and 91.9°. In 1990, Pope et al.[17] performed an MCSCF study on the $\tilde{X}$ state and obtained r_e and θ_e values of 1.442 Å and 92.9°. The most recent theoretical study (1994), by Austen, Eriksson, and Boyd,[59] used density functional theory to investigate PH_2 and predicted r_e and θ_e to be 1.437 Å and 90.6°.

Regarding theoretically predicted geometries, it is important to recognize the trends imposed by both the size of the basis set and the level of correlation achieved. Larger basis sets generally tend to contract bond distances, while more complete treatments of electron correlation usually lengthen bonds.[57,58] Predicted geometries for the three lowest-lying states of PH_2, at four levels of theory with the cc-pVQZ basis set, are depicted in Figures 1-3.

At the CCSD(T)/TZ3P(2f,2d)+2diff level of theory (highest level of theory employeed in ref 3), the equilibrium bond length (r_e) of the $\tilde{X}\ ^2B_1$ state of PH_2 was predicted to be 1.4188 Å, and the bond angle (θ_e) was predicted to be 91.79°. This bond angle is significantly smaller (by ∼11°) than the predicted bond angle (103.33°) for the isovalent $\tilde{X}\ ^2B_1$ NH_2 molecule at the same level of theory.[3] This trend is also seen for the $\tilde{A}\ ^2A_1$ state. The latter θ_e value (121.82°) of PH_2 is much smaller (by ∼23°) than that for the $\tilde{A}\ ^2A_1$ state of NH_2 (145.08°) at the same level of theory. The difference in the magnitudes of the bond angles in NH_2 and PH_2 may be qualitatively explained by the reduced hybridizing ability of the valence orbitals (3s and 3p) of the phosphorus atom.

The most reliable level of theory, CCSD(T)/cc-pVQZ, of the present study predicts the equilibrium structure for the $\tilde{X}\ ^2B_1$ state to be $r_e = 1.4200$ Å and $\theta_e = 91.87°$. These values agree

TABLE 6: Theoretical Predictions of the Total Energy (in hartree), Bond Length (in Å), Bond Angle (in deg), P···H_2 Length (in Å), Harmonic Vibrational Frequencies (in cm^{-1}), and Zero-Point Vibrational Energy (in kcal/mol) for the $\tilde{B}\ ^2B_2$ State of the PH_2 Molecule at the CCSD and CCSD(T) Levels of Theory

level of theory	energy	r_e	$r_{P\cdots H_2}$	θ_e	$\omega_1(a_1)$	$\omega_2(a_1)$	$\omega_3(b_2)$	ZPVE
TZ2P CCSD	−341.906233	1.7153	1.6669	27.30	3409	701	1307	7.75
TZ2P+diff CCSD	−341.907320	1.7139	1.6653	27.35	3401	710	1311	7.75
TZ3P CCSD	−341.910494	1.6783	1.6278	28.18	3311	831	1435	7.97
TZ3P+2diff CCSD	−341.911560	1.6776	1.6270	28.21	3307	837	1433	7.97
TZ2P(f,d) CCSD	−341.926741	1.6819	1.6313	28.17	3296	815	1429	7.92
TZ2P(f,d)+diff CCSD	−341.927746	1.6808	1.6300	28.23	3288	823	1434	7.93
TZ3P(2f,2d) CCSD	−341.932636	1.6656	1.6141	28.59	3250	886	1477	8.02
TZ3P(2f,2d)+2diff CCSD	−341.933355	1.6653	1.6136	28.61	3247	891	1478	8.03
cc-pVDZ CCSD	−341.884095	1.7538	1.7057	26.90	3542	658	1274	7.83
cc-pVTZ CCSD	−341.934604	1.6854	1.6351	28.08	3315	827	1437	7.98
cc-pVQZ CCSD	−341.947666	1.6685	1.6170	28.53	3257	885	1489	8.05
TZ2P CCSD(T)	−341.910688	1.6960	1.6459	27.92	3300	747	1376	7.75
TZ2P+diff CCSD(T)	−341.911848	1.6951	1.6449	27.96	3292	753	1378	7.75
TZ3P CCSD(T)	−341.915694	1.6653	1.6134	28.70	3213	864	1489	7.96
TZ3P+2diff CCSD(T)	−341.916827	1.6649	1.6129	28.72	3210	869	1486	7.96
TZ2P(f,d) CCSD(T)	−341.932932	1.6677	1.6156	28.74	3190	849	1488	7.90
TZ2P(f,d)+diff CCSD(T)	−341.933987	1.6671	1.6148	28.78	3182	855	1492	7.90
TZ3P(2f,2d) CCSD(T)	−341.939785	1.6540	1.6009	29.11	3147	914	1530	7.99
TZ3P(2f,2d)+2diff CCSD(T)	−341.940543	1.6538	1.6007	29.13	3145	917	1530	7.99
cc-pVDZ CCSD(T)	−341.887085	1.7371	1.6877	27.39	3443	704	1302	7.79
cc-pVTZ CCSD(T)	−341.941148	1.6716	1.6198	28.62	3202	883	1465	7.93
cc-pVQZ CCSD(T)	−341.955388	1.6563	1.6033	29.08	3150	913	1543	8.01

TABLE 7: Theoretical Predictions of the Total CASSCF and CASSCF-SOCI Energies (in hartree) at the CISD-Optimized Geometries

level of theory	state	CSFs	energy
TZ2P CASSCF	$\tilde{X}\ ^2B_1$	588	−341.938741
TZ3P CASSCF	$\tilde{X}\ ^2B_1$	588	−341.940429
TZ2P(f,d) CASSCF	$\tilde{X}\ ^2B_1$	588	−341.940378
TZ3P(2f,2d) CASSCF	$\tilde{X}\ ^2B_1$	588	−341.941844
TZ2P CASSCF	$\tilde{A}\ ^2A_1$	616	−341.852414
TZ3P CASSCF	$\tilde{A}\ ^2A_1$	616	−341.854642
TZ2P(f,d) CASSCF	$\tilde{A}\ ^2A_1$	616	−341.854523
TZ3P(2f,2d) CASSCF	$\tilde{A}\ ^2A_1$	616	−341.856438
TZ2P CASSCF	$\tilde{B}\ ^2B_2$	588	−341.820685
TZ3P CASSCF	$\tilde{B}\ ^2B_2$	588	−341.822320
TZ2P(f,d) CASSCF	$\tilde{B}\ ^2B_2$	588	−341.824123
TZ3P(2f,2d) CASSCF	$\tilde{B}\ ^2B_2$	588	−341.826309
TZ2P CASSCF-SOCI	$\tilde{X}\ ^2B_1$	407 398	−342.028082
TZ3P CASSCF-SOCI	$\tilde{X}\ ^2B_1$	694 614	−342.031852
TZ2P(f,d) CASSCF-SOCI	$\tilde{X}\ ^2B_1$	883 488	−342.047688
TZ3P(2f,2d) CASSCF-SOCI	$\tilde{X}\ ^2B_1$	2 064 412	−342.052738
TZ2P CASSCF-SOCI	$\tilde{A}\ ^2A_1$	408 656	−341.942163
TZ3P CASSCF-SOCI	$\tilde{A}\ ^2A_1$	696 316	−341.946633
TZ2P(f,d) CASSCF-SOCI	$\tilde{A}\ ^2A_1$	885 244	−341.962572
TZ3P(2f,2d) CASSCF-SOCI	$\tilde{A}\ ^2A_1$	2 067 272	−341.968480
TZ2P CASSCF-SOCI	$\tilde{B}\ ^2B_2$	408 158	−341.909282
TZ3P CASSCF-SOCI	$\tilde{B}\ ^2B_2$	695 670	−341.914061
TZ2P(f,d) CASSCF-SOCI	$\tilde{B}\ ^2B_2$	884 544	−341.930812
TZ3P(2f,2d) CASSCF-SOCI	$\tilde{B}\ ^2B_2$	2 066 204	−341.937263

TABLE 8: Relative Energies T_e (T_0 in Parentheses) in kcal/mol for the Three Lowest-Lying Electronic States of PH_2 at the SCF, CASSCF, CISD, and CASSCF-SOCI Levels of Theory

level of theory	$\tilde{X}\ ^2B_1$	$\tilde{A}\ ^2A_1$	$\tilde{B}\ ^2B_2$
TZ2P SCF	0.0	54.29(54.48)	75.63(74.60)
TZ2P+diff SCF	0.0	54.21(54.40)	75.41(74.42)
TZ3P SCF	0.0	54.45(54.61)	76.42(75.40)
TZ3P+2diff SCF	0.0	54.26(54.42)	76.14(75.15)
TZ2P(f,d) SCF	0.0	53.81(53.98)	75.39(74.43)
TZ2P(f,d)+diff SCF	0.0	53.79(53.96)	75.17(74.25)
TZ3P(2f,2d) SCF	0.0	53.89(54.06)	75.44(74.56)
TZ3P(2f,2d)+2diff SCF	0.0	53.73(53.90)	75.20(74.33)
cc-pVDZ SCF	0.0	55.43(55.61)	75.53(74.62)
cc-pVTZ SCF	0.0	54.12(54.30)	74.93(74.04)
cc-pVQZ SCF	0.0	53.77(53.94)	74.92(74.07)
TZ2P CASSCF	0.0	54.17(54.41)	74.08(73.40)
TZ3P CASSCF	0.0	53.83(53.99)	74.11(73.53)
TZ2P(f,d) CASSCF	0.0	53.87(54.04)	72.95(72.36)
TZ3P(2f,2d) CASSCF	0.0	53.59(53.74)	72.50(71.98)
TZ2P CISD	0.0	53.98(54.22)	75.29(74.61)
TZ2P+diff CISD	0.0	53.89(54.12)	75.05(74.38)
TZ3P CISD	0.0	53.78(53.94)	75.01(74.43)
TZ3P+2diff CISD	0.0	53.63(53.79)	74.66(74.08)
TZ2P(f,d) CISD	0.0	53.48(53.65)	74.39(73.80)
TZ2P(f,d)+diff CISD	0.0	53.45(53.61)	74.16(73.57)
TZ3P(2f,2d) CISD	0.0	53.15(53.30)	73.80(73.28)
TZ3P(2f,2d)+2diff CISD	0.0	53.02(53.16)	73.57(73.05)
cc-pVDZ CISD	0.0	55.54(55.72)	76.65(75.99)
cc-pVTZ CISD	0.0	53.41(53.56)	73.59(73.05)
cc-pVQZ CISD	0.0	52.72(52.87)	73.22(72.72)
TZ2P CASSCF-SOCI	0.0	53.92(54.16)	74.55(73.87)
TZ3P CASSCF-SOCI	0.0	53.48(53.64)	73.92(73.34)
TZ2P(f,d) CASSCF-SOCI	0.0	53.41(53.58)	73.34(72.75)
TZ3P(2f,2d) CASSCF-SOCI	0.0	52.87(53.02)	72.46(71.94)
expt refs 8,22		(52.26)	
expt refs 23,24		(52.08)	

well with the recent microwave spectroscopic results obtained by Hirao et al.[20] and suggest that the amount of electron correlation included at this level of theory is sufficient to predict accurate molecular structures. Our equilibrium structure r_e = 1.3948 Å and θ_e = 121.88° at the highest level of theory for the $\tilde{A}$ state is also consistent with the experimental structures[18,19] and reaffirms the reliability of this level of theory.

The second excited electronic state ($\tilde{B}\ ^2B_2$) of PH_2 is characterized by its acute bond angle of 29.08° and a substantially elongated r_e of 1.6563 Å with the CCSD(T)/cc-pVQZ method. Unfortunately, there is no experimental structure available to date. This state may be considered to be a T-shaped complex, with P···H_2 describing the system more appropriately. The distance between P and the center of the two H atoms is 1.6033 Å, and the distance between the two H atoms is 0.8317 Å. The equilibrium bond length of isolated H_2 is experimentally determined[60] to be 0.7414 Å. Thus, the H−H distance in the $\tilde{B}$ state is significantly elongated compared to the isolated H_2 molecule. The H−H distance increases with improved treatment of correlation effects, whereas the P···H_2 distance decreases with correlation effects. These features indicate a stronger P···H_2 interaction due to the inproved dynamical correlation treatment.

B. Dipole Moments. The theoretical dipole moments of the ground state of PH_2 in Table 1 decrease with inclusion of correlation effects. The addition of higher angular momentum

TABLE 9: Relative Energies T_e (T_0 in Parentheses) in kcal/mol for the Three Lowest-Lying Electronic States of PH_2 at the CCSD and CCSD(T) Levels of Theory

level of theory	$\tilde{X}\ ^2B_1$	$\tilde{A}\ ^2A_1$	$\tilde{B}\ ^2B_2$
TZ2P CCSD	0.0	53.85(54.10)	74.76(74.09)
TZ2P+diff CCSD	0.0	53.74(53.97)	74.50(73.82)
TZ3P CCSD	0.0	53.52(53.69)	74.35(73.77)
TZ3P+2diff CCSD	0.0	53.37(53.53)	73.98(73.40)
TZ2P(f,d) CCSD	0.0	53.35(53.52)	73.78(73.19)
TZ2P(f,d)+diff CCSD	0.0	53.31(53.47)	73.54(72.95)
TZ3P(2f,2d) CCSD	0.0	52.88(53.02)	73.07(72.54)
TZ3P(2f,2d)+2diff CCSD	0.0	52.75(52.89)	72.83(72.31)
cc-pVDZ CCSD	0.0	55.55(55.75)	76.31(75.65)
cc-pVTZ CCSD	0.0	53.21(53.37)	72.92(72.39)
cc-pVQZ CCSD	0.0	52.45(52.60)	72.49(72.00)
TZ2P CCSD(T)	0.0	53.73(53.98)	74.53(73.89)
TZ2P+diff CCSD(T)	0.0	53.60(53.84)	74.25(73.61)
TZ3P CCSD(T)	0.0	53.26(53.43)	73.86(73.31)
TZ3P+2diff CCSD(T)	0.0	53.09(53.25)	73.47(72.92)
TZ2P(f,d) CCSD(T)	0.0	53.10(53.27)	73.29(72.71)
TZ2P(f,d)+diff CCSD(T)	0.0	53.04(53.20)	73.04(72.46)
TZ3P(2f,2d) CCSD(T)	0.0	52.46(52.60)	72.35(71.83)
TZ3P(2f,2d)+2diff CCSD(T)	0.0	52.32(52.46)	72.09(71.57)
cc-pVDZ CCSD(T)	0.0	55.58(55.79)	76.27(75.62)
cc-pVTZ CCSD(T)	0.0	52.91(53.07)	72.39(71.87)
cc-pVQZ CCSD(T)	0.0	52.03(52.19)	71.74(71.28)
expt refs 8,22		(52.26)	
expt refs 23,24		(52.08)	

functions to the basis set generally decreases the dipole moment, whereas the augmentation of the basis set with diffuse functions increases it. At the highest CISD level of theory, CISD/TZ3P-(2f,2d)+2diff, the dipole moment of the ground state is predicted to be 0.570 D. This is significantly smaller than the dipole moment of 1.804 D for the ground-state NH_2 at the same level of theory.[3] This disparity may be attributed largely to the difference in electronegativity of nitrogen (3.1) and phosphorus (2.1) atoms. Because of the wider bond angle in the $\tilde{A}\ ^2A_1$ state of PH_2, the dipole moment is substantially smaller than that of the ground state; with the same method, it is determined to be 0.364 D. Again, there is a significant difference between the dipole moments of PH_2 and NH_2 (0.672 D) for the $\tilde{A}\ ^2A_1$ states.[3] The influences of correlation effects and addition of diffuse functions to the basis set are similar to those observed in the ground state. At the CISD/TZ3P(2f,2d)+2diff level of theory, the dipole moment of the $\tilde{B}\ ^2B_2$ small angle state is predicted to be 1.500 D. Contrary to the previous cases, the dipole moment increases upon introduction of electron correlation. There is a substantial difference between the dipole moment of the $\tilde{B}$ state of NH_2 (2.619 D) and that of the $\tilde{B}$ state of PH_2 (1.500 D). The magnitude of the dipole moment of this small angle state is the largest among the three PH_2 states studied. The electrons occupying the $5a_1$ orbital (along the C_2 axis) appear to enhance the polarity of the molecule, as evidenced by the dipole moments for the $\tilde{X}\ ^2B_1$ state ($\mu_e = 0.570$ D) and the $\tilde{B}\ ^2B_2$ state ($\mu_e = 1.500$ D).

C. Harmonic Vibrational Frequencies. The fundamental vibrational frequencies for the ground state $\tilde{X}\ ^2B_1$ of PH_2 have been experimentally measured to be $\nu_1 = 2270 \pm 80$ cm^{-1} by laser photoelectron spectroscopy,[61] $\nu_2 = 1102$ cm^{-1} by UV spectroscopy,[18] $\nu_1 = 2310$ cm^{-1} by high-temperature Raman spectroscopy,[21] and $\nu_2 = 1103$ cm^{-1} by IR methods in an argon medium.[22] The ν_3 mode has not been observed. The newly predicted harmonic vibrational frequencies with the CCSD(T)/cc-pVQZ method in the present study are 2396 cm^{-1} (ω_1), 1125 cm^{-1} (ω_2), and 2404 cm^{-1} (ω_3). Thus, ω_1 and ω_3 are predicted to be remarkably close. Theoretical harmonic vibrational frequencies for small molecules at the CCSD(T) level with a TZ2P(f,d) basis set provide values typically 5% above the experimental fundamental frequencies.[57,58,62] Considering this general tendency, the theoretical (harmonic) and experimental (fundamental) vibrational frequencies are reasonably consistent.

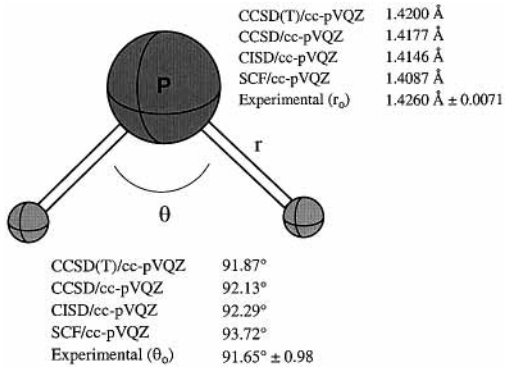

Figure 1. Predicted geometries (r_e and θ_e values) of the $\tilde{X}\ ^2B_1$ state of PH_2 at four levels of theory with the cc-pVQZ basis set.

The theoretical stretching harmonic frequencies (ω_1 and ω_3) for the first excited state $\tilde{A}\ ^2A_1$ are predicted to be 2483 and 2584 cm^{-1}, respectively. These (ω_1 and ω_3) vibrational frequencies are significantly higher relative to those for the ground state, due to the shorter (about 2%) PH bond length. This feature is in accord with Badger's rule[63,64] that a shorter bond length provides a larger force constant (a higher frequency). On the other hand, the bending frequency (ω_2) is lower than that of the ground-state, owing to the wider bond angle of the $\tilde{A}\ ^2A_1$ state. The bending frequency was measured to be 949 cm^{-1} (ν_2) by both UV spectroscopy[21] and solid argon absorption studies.[22,23] The corresponding theoretical harmonic frequency, at the CCSD(T)/cc-pVQZ level, is predicted to be 968 cm^{-1}. As mentioned in subsection A, the $\tilde{B}\ ^2B_2$ state of PH_2 may be regarded as a T-shaped structure or a P···H_2 complex. Thus, the harmonic vibrational frequencies for this state may be assigned as $\omega_1 = 3150$ cm^{-1} (a_1, HH stretch), $\omega_2 = 913$ cm^{-1} (a_1, PH_2 symmetric stretch), and $\omega_3 = 1543$ cm^{-1} (b_2, PH_2 asymmetric stretch), respectively. The experimental harmonic vibrational frequencies of H_2 and H_2^+ are 4401 and 2322 cm^{-1}, respectively.[60] The frequency of the ω_1 mode for the $\tilde{B}\ ^2B_2$ state of PH_2 is therefore smaller than that of H_2 but significantly larger than that of H_2^+.

D. Infrared (IR) Intensities. For the $\tilde{X}\ ^2B_1$ state of PH_2 the asymmetric stretching mode (ω_3) shows a larger IR intensity than the symmetric stretching mode (ω_1). In comparison to the ground state, the three IR intensities for the $\tilde{A}\ ^2A_1$ state are much smaller. For the $\tilde{B}\ ^2B_2$ state of PH_2, the IR intensities of the three vibrational modes show a large disparity between the SCF level of theory and the more accurate CISD method. These large changes in intensities were expected due to the vast differences in $\tilde{B}\ ^2B_2$ geometrical parameters which resulted from the additional correlation treatment in the CISD method.

E. Energetics. *1.* $\tilde{X}\ ^2B_1$–$\tilde{A}\ ^2A_1$ *Splitting.* The energy separation (T_0 value) between the ground and first excited state has been experimentally determined to be 52.26 kcal/mol (2.266 eV, 18276.59 cm^{-1})[8,22] and 52.08 kcal/mol (2.258 eV, 18215 cm^{-1})[23,24] via gas-phase and argon matrix studies. This energy gap is reproduced well at all levels of theory as shown in Tables 8 and 9. With the largest basis set used, $\tilde{X}$–$\tilde{A}$ splittings (T_0 values) are predicted to be 53.9 kcal/mol [SCF], 53.7 kcal/mol [CASSCF], 52.9 kcal/mol [CISD], 53.0 kcal/mol [CASSCF-SOCI], 52.6 kcal/mol [CCSD], and 52.2 kcal/mol [CCSD(T)]. Peric at al.[15] reported this energy splitting to be 53.8 kcal/mol which was a significant improvement over the 65.3 kcal/mol predicted by an early SCF study.[13] Our best T_0 value of 52.2

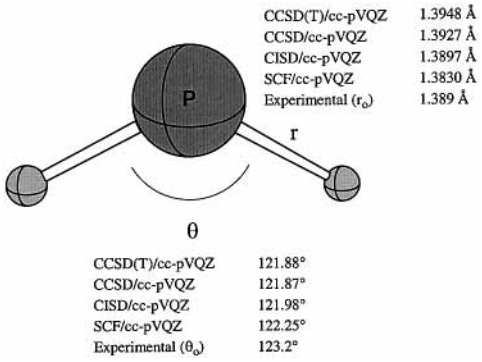

Figure 2. Predicted geometries (r_e and θ_e values) of the $\tilde{A}\ ^2A_1$ state of PH_2 at four levels of theory with the cc-pVQZ basis set.

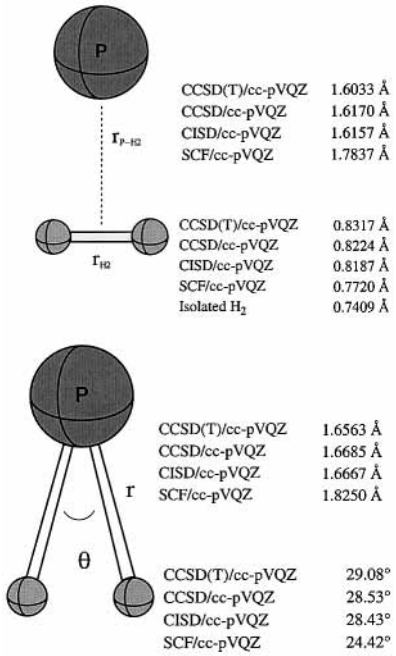

Figure 3. Predicted geometries (r_e and θ_e values) of the $\tilde{B}\ ^2B_2$ state of PH_2 at four levels of theory with the cc-pVQZ basis set.

kcal/mol (2.26 eV, 18 300 cm^{-1}) is further improved and is in excellent agreement with the experimental values of 18 277 cm^{-1} [8,22] and 18 215 cm^{-1}.[23,24] It is clearly seen that advanced treatments of correlation effects and expansion of basis sets enhance the agreement between theoretical predictions and experimental observation.

2. $\tilde{A}\ ^2B_1-\tilde{B}\ ^2B_2$ *Splitting.* The T_0 value for the $\tilde{X}-\tilde{B}$ splitting has not been determined experimentally. Our theoretical energy splittings (T_0 values) show a pattern of convergence with increasing level of correlation and basis set size. Our values with the largest basis set are as follows: 74.1 kcal/mol [SCF], 72.0 kcal/mol [CASSCF], 72.7 kcal/mol [CISD], 71.9 kcal/mol [CASSCF-SOCI], 72.0 kcal/mol [CCSD], and 71.3 kcal/mol [CCSD(T)]. The most reliable T_0 value for the $\tilde{X}-\tilde{B}$ splitting 71.3 kcal/mol (3.09 eV, 24 900 cm^{-1}) is expected to be within a chemical accuracy of $\pm$ 1 kcal/mol.

It should be noted that we do not observe variational collapse owing to instability of the wave functions of the $\tilde{A}\ ^2A_1$ and $\tilde{B}\ ^2B_2$ excited states in asymmetrically distorted geometries, i.e., in C_s symmetry. This is because the vast geometrical changes observed between the ground and excited states lead to only one lower-lying state ($\tilde{X}\ ^2B_1$).

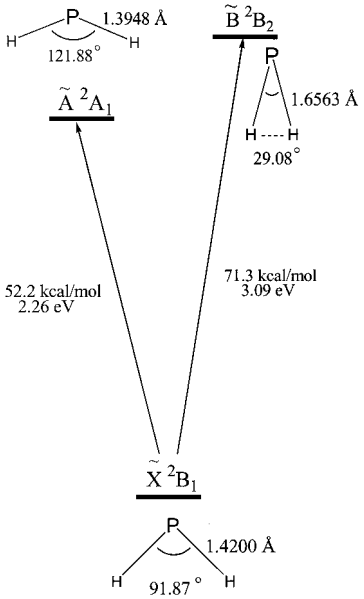

Figure 4. State diagram showing energy separations (in kcal/mol and eV) and geometries (r_e and θ_e) of the $\tilde{X}\ ^2B_1$, $\tilde{A}\ ^2A_1$, and $\tilde{B}\ ^2B_2$ states of PH_2 at the CCSD(T)/cc-pVQZ level of theory.

5. Concluding Remarks

The three lowest-lying electronic states $\tilde{X}\ ^2B_1$, $\tilde{A}\ ^2A_1$, and $\tilde{B}\ ^2B_2$ of the PH_2 radical have been systematically studied using ab initio electronic structure theory. It was found that the energetics and physical properties of the three equilibrium states investigated in the present study may be correctly obtained at all levels of theory in the variational sense. The theoretically predicted equilibrium structures and physical properties agree quite well with the available experimental values. The newly predicted geometrical parameters for the $\tilde{B}\ ^2B_2$ state of PH_2 are $r_e = 1.6563$ Å and $\theta_e = 29.08°$.

The $\tilde{X}\ ^2B_1-\tilde{A}\ ^2A_1$ energy separation is predicted to be 52.2 kcal/mol (2.26 eV, 18 300 cm^{-1}), which is in excellent agreement with the experimental values of 52.26 kcal/mol (2.266 eV, 18 276.59 cm^{-1})[8,22] and 52.08 kcal/mol (2.258 eV, 18 215 cm^{-1}).[23,24] The second excited state is determined to lie 71.3 kcal/mol (3.09 eV, 24 900 cm^{-1}) above the ground state. A state diagram showing energy separations and geometries of the three lowest-lying states of PH_2 at the CCSD(T)/cc-pVQZ level of theory is presented in Figure 4. It is hoped that the present study would help to detect the $\tilde{B}\ ^2B_2$ state with its acute bond angle, although traditional routes to its formation undoubtedly will be hampered by poor Franck−Condon overlap with the ground or first excited state. It is demonstrated that by employing highly correlated wave functions and large basis sets, the energetic predictions reach a chemical accuracy of $\pm$ 1 kcal/mol.

Acknowledgment. We would like to thank Dr. T. V. Huis for helpful scientific discussion. This research was supported by the National Science Foundation Grant CHE-981539.

References and Notes

(1) Okumura, M.; Yeh, L.; Normand, D.; Vandenbiesen, J. J. H.; Bustamente, S. W.; Lee, Y. T.; Lee, T. J.; Handy, N. C.; Schaefer, H. F. *J. Chem. Phys.* **1987**, *86*, 3807.

(2) Olsen, J.; Jørgensen, P.; Koch, H.; Balkova, A.; Bartlett, R. *J. Chem. Phys.***1996**, *104*, 8007.

(3) Yamaguchi, Y.; Hoffman, B. C.; Stephens, J. C.; Schaefer, H. F. *J. Phys. Chem. A* **1999**, *103*, 7701.

(4) Stringfellow, G. B. In *Organometalic Vapor-Phase Epitaxy: Theory and Practice*; Academic Press: New York, 1998.

(5) Kampas, F. J. In *Semiconductors and Semimetals*; Pankove, J. I., Ed.; Academic Press: New York, 1984; Vol. 2.
(6) Lee, J. H.; Michael, J. V.; Payne, W. A.; Whytlock, D. A.; Stief, L. J. *J. Chem. Phys*. **1976**, *65*, 3280.
(7) Prinn, R. G.; Lewis, J. S. *Science* **1975**, *190*, 274.
(8) Ramsay, D. A. *Nature (London)* **1956**, *178*, 374.
(9) Guenebaut, H.; Pascat, B. *Compt. Rend. Acad. Sci. (Paris)* **1964**, *259*, 2412.
(10) Dixon, R. N.; Duxbury, G.; Ramsay, D. A. *Proc. R. Soc. London, Ser. A* **1967**, *296*, 137.
(11) Davies, P. B.; Russell, D. K.; Thrush, B. A.; Radford, H. E. *Chem. Phys.* **1979**, *44*, 421.
(12) Dixon, R. N. *Trans. Faraday. Soc.* **1964**, *60*, 1363.
(13) So, S. P.; Richards, W. G. *Int. J. Quantum Chem.* **1977**, *9*, 73.
(14) Ball, J. R.; Thomson, C. *Int. J. Quantum Chem.* **1978**, *14*, 39.
(15) Peric, M.; Buenker, R. J.; Peyerimhoff, S. D. *Can. J. Chem.* **1979**, *57*, 2491.
(16) Alberts, I. L.; Handy, N. C. *J. Chem. Phys.* **1988**, *89*, 2107.
(17) Pope, S. A.; Miller, I. H.; Guest, M. F. *Faraday Symp. Chem. Soc*. **1990**, *19*, 109.
(18) Herzberg, G. *Molecular Spectra and Molecular Structure*; Van Nostrand Reinhold: New York, 1966; Vol. III.
(19) Berthou, M. Ph. D Thesis, Universite de Reims, Reims, France, 1971.
(20) Hirao, T.; Hayakashi, S.; Yamamoto, S.; Saito, S. *J. Mol. Spectrosc.* **1998**, *187*, 153.
(21) P. Abraham; A. Bekkaoui; J. Bouix; Y. Monteil, *J. Raman Spectosc.* **1992**, *23*, 279.
(22) Berthou, M.; Pascat, B.; Guenebaut, H.; Ramsay, D. A. *Can. J. Phys.* **1972**, *50*, 2265.
(23) Larzilliere, M.; Jacox, M. E. *Proc. 10th Mater. Res. Symp. Characterization High Temp. Vapors Gases* **1979**, *561*, 529.
(24) Withall, R.; McCluskey, M.; Andrews, L. *J. Phys. Chem.* **1989**, *93*, 126.
(25) Van Huis, T. J.; Yamaguchi, Y.; Sherrill, C. D.; Schaefer, H. F. *J. Phys. Chem. A* **1997**, *101*, 6955.
(26) Mclean, A. D.; Chandler, G. S. *J. Chem. Phys*. **1980**, *72*, 5639.
(27) Huzinaga, S. *Approximate Atomic Wavefunctions*; Department of Chem.: University of Alberta, 1971; Vol. II.
(28) Dunning, T. H. *J. Chem. Phys.* **1971**, *55*, 716.
(29) Huzinaga, S. *J. Chem. Phys*. **1965**, *42*, 1293.
(30) Lee, T. J.; Schaefer, H. F. *J. Chem. Phys.* **1985**, *83*, 1784.
(31) Dunning, T. H. *J. Chem. Phys.* **1989**, *90*, 1007.
(32) Woon, D. E.; Dunning, T. H. *J. Chem. Phys.* **1995**, *103*, 4572.
(33) Pulay, P. *Mol. Phys.* **1969**, *17*, 197.
(34) Pulay, P. In *Modern Theoretical Chemistry*; Schaefer, H. F., Ed.; Plenum Press: New York. 1977; Vol. 4, 153−185.
(35) Yamaguchi, Y.; Osamura, Y.; Goddard, J. D.; Schaefer, H. F. *A New Dimension to Quantum Chemistry: Analytic Derivative Methods in ab Initio Molecular Electronic Structure Theory*; Oxford University Press: New York, 1994.
(36) Purvis, G. D.; Bartlett, R. J. *J. Chem. Phys.* **1982**, *76*, 1910.
(37) Raghavachari, K.; Trucks, G. W.; Pople, J. A.; Head-Gordon, M. *Chem. Phys. Lett.* **1989**, *157*, 479.
(38) Scuseria, G. E. *Chem. Phys. Lett.* **1991**, *176*, 27.
(39) Siegbahn, P. E. M.; Heiberg, A.; Roos, B. O.; Levy, B. *Phys. Scr.* **1980**, *21*, 323.
(40) Roos, B. O.; Taylor, P. R.; Siegbahn, P. E. M. *Chem. Phys.* **1980**, *48*, 157.
(41) Roos, B. O. *Int. J. Quantum Chem.* **1980**, *14*, 175.
(42) Schaefer, H. F. Ph.D. Thesis, Department of Chemistry, Stanford University, Palo Alto, CA, 1969.
(43) Saxe, P.; Yamaguchi, Y.; Schaefer, H. F. *J. Chem. Phys.* **1982**, *77*, 5647.
(44) Osamura, Y.; Yamaguchi, Y.; Saxe, P.; Vincent, M. A.; Gaw, J. F.; Schaefer, H. F. *Chem. Phys.* **1982**, *72*, 131.
(45) Osamura, Y.; Yamaguchi, Y.; Saxe, P.; Fox, D. J.; Vincent, M. A.; Schaefer, H. F. *J. Mol. Struct.* **1983**, *103*, 183.
(46) Yamaguchi. Y.; Frisch, M. J.; Lee, T. J.; Schaefer, H. F.; Binkley, J. S. *J. Chem. Phys.* **1986**, *69*, 337.
(47) Brooks, B. R.; Laidig, W. D.; Saxe, P.; Goddard, J. D.; Yamaguchi, Y.; Schaefer, H. F. *J. Chem. Phys.* **1980**, *72*, 4652.
(48) Rice, J. E.; Amos, R. D.; Handy, N. C.; Lee, T. J.; Schaefer, H. F. *J. Chem. Phys.* **1986**, *85*, 963.
(49) Lee, T. J.; Allen, W. D.; Schaefer, H. F. *J. Chem. Phys.* **1987**, *87*, 7062.
(50) Allen, W. D.; Schaefer, H. F. *J. Chem. Phys.* **1987**, *87*, 7076.
(51) King, R. A.; Schaefer, H. F. *Spectrochim. Acta, Part A* **1997**, *53*, 1163.
(52) Janssen, C. L.; Seidl, T. E.; Scuseria, G. E.; Hamilton, T. P.; Yamaguchi, Y.; Remington, R. B.; Xie, Y.; Vacek, G.; Sherrill, C. D.; Crawford, T. D.; Fermann, J. T.; Allen, W. D.; Brooks, B. R.; Fitzgerald, G. B.; Fox, D. J.; Gaw, J. F.; Handy, N. C.; Laidig, W. D.; Lee. T. J.; Pitzer, R. M.; Rice, J. E.; Saxe, P.; Scheiner, A. C.; Schaefer, H. F. PSI 2.0.8; PSITECH, Inc.: Watkinsville, GA, 1994.
(53) Walsh, A. D. *J. Chem. Soc.* **1953**, 2260.
(54) Yamaguchi, Y.; Alberts, I. L.; Goddard, J. D.; Schaefer, H. F. *Chem. Phys.* **1990**, *147*, 309.
(55) Hinchcliffe, A.; Bounds, D. G. *J. Mol. Struct.* **1979**, *54*, 231.
(56) Peric, M.; Runau, R.; Romelt, J.; Peyerimhoff, S. D. *J. Mol. Spectrosc.* **1979**, *78*, 309.
(57) Yamaguchi, Y.; Schaefer, H. F. *J. Chem. Phys.* **1980**, *73*, 2310.
(58) Thomas, J. R.; DeLeeuw, B. J.; Vacek, G.; Crawford, T. D.; Yamaguchi, Y.; Schaefer, H. F. *J. Chem. Phys.* **1993**, *99*, 403.
(59) Austen, M. A.; Eriksson, L. A.; Boyd, R. J. *Can. J. Chem.* **1994**, *72*, 453.
(60) Huber, K. P.; Herzberg, G. *Molecular Spectra and Molecular Structure. IV. Constants of Diatomic Molecules*; Van Nostrand Reinhold: New York, New York, 1979.
(61) Zittel, P. F.; Lineberger, W. C. *J. Chem. Phys.* **1976**, *65*, 1236.
(62) Besler, B.; Scuseria, G. E.; Scheiner, A. C.; Schaefer, H. F. *J. Chem. Phys.* **1988**, *89*, 360.
(63) Badger, R. M. *J. Chem. Phys.* **1934**, *2*, 128.
(64) Badger, R. M. *J. Chem. Phys.* **1935**, *3*, 710.